

Coupling Finite Element based Models and Machine Learning to Recreate Aortic Wall Mechanics

André Mourato^{a,b,*}, Rodrigo Valente^{a,b}, José Xavier^{a,b,**}, Moisés Brito^{a,b}, Stéphane Avril^c, António C. Tomás^d and José Fragata^{d,e}

^aUNIDEMI, Department of Mechanical and Industrial Engineering, NOVA School of Science and Technology, Universidade NOVA de Lisboa, Campus da Caparica, Caparica 2829-516, Portugal

^bIntelligent Systems Associate Laboratory, Campus Azurém, Guimarães 4800-058, Portugal

^cÉcole des Mines de Saint-Étienne, University of Lyon, Inserm, Sainbiose U1059, Centre Ingénierie et Santé 10, rue de la Marandière, Saint-Etienne F-42270, France

^dDepartment of Cardiothoracic Surgery, Santa Marta Hospital, Rua de Santa Marta 50, Lisboa 1169-024, Portugal

^eDepartment of Surgery and Human Morphology, NOVA Medical School, Universidade NOVA de Lisboa, Campo Mártires da Pátria 130, Lisboa 1169-056, Portugal

ARTICLE INFO

Keywords:

Ascending Thoracic Aortic Aneurysm (ATAA)

Computational Solid Mechanics (CSM)

Deep Learning (DL)

Patient-specific

Surrogate modelling

ABSTRACT

Background and Objective: Ascending Thoracic Aortic Aneurysms (ATAAs) require accurate biomechanical assessment. However, current numerical approaches are too computationally demanding for routine clinical use. This work proposes a Deep Neural Networks (DNN)-based surrogate model to overcome this limitation.

Methods: A Statistical Shape Model (SSM) was developed from a dataset of patient-specific ascending aortas. The global anatomical derived from the Principal Component Analysis (PCA), coupled with material and loading parameters, were used as inputs for a DNN. The network was trained to predict stress and strain fields, using Computational Solid Mechanics (CSM) simulations as reference. Model performance was assessed both on synthetic PCA-driven geometries and on the original patient-specific anatomies.

Results: The surrogate model reproduced the spatial distributions of the Second Piola-Kirchhoff and Right Green-Cauchy fields with high reliability. For PCA-driven geometries, around 99% of the test cases achieved at least moderate agreement with reference simulations. For patient-specific anatomies, more than 95 % of the predictions showed at least moderate agreement. Errors were mainly associated with low-pressure loading conditions, while no clear dependency was found on shape or material inputs.

Conclusions: The results highlight the potential of data-driven approaches to accelerate patient-specific biomechanical assessments, paving the way for integration into future clinical decision-support systems.

1. Introduction

Ascending Thoracic Aortic Aneurysms (ATAAs) represent a risk factor for the development of life-threatening cardiovascular events, such as aortic dissection or rupture [1, 2]. The clinical guidelines for the diagnosis and treatment of aortic aneurysms rely on the maximum aortic diameter as a primary risk stratification criterion [3, 4]. However, this metric fails to capture patient-specific biomechanical factors known to influence aortic wall failure [5, 6]. Numerical models are fundamental tools in engineering, enabling the analysis of complex systems. More recently, numerical models have been increasingly applied in the field of cardiovascular biomechanics [7–10] as alternatives to traditional risk stratification methods. One significant limitation of numerical modelling, in particular for clinical applications, is that it usually requires extensive reporting times. Additionally, it also often requires running multiple simulations.

*Corresponding author

**Principal corresponding author

✉ af.mourato@campus.fct.unl.pt (A. Mourato); rb.valente@campus.fct.unl.pt (R. Valente); jmc.xavier@fct.unl.pt (J. Xavier); moisesbrito@fct.unl.pt (M. Brito); avril@emse.fr (S. Avril); acruzomas@gmail.com (A.C. Tomás); jose.fragata@nms.unl.pt (J. Fragata)

ORCID(s): 0000-0002-2996-1951 (A. Mourato); 0000-0003-0871-0683 (R. Valente); 0000-0002-7836-4598 (J. Xavier); 0000-0002-7024-9958 (M. Brito); 0000-0002-8604-7736 (S. Avril); 0000-0002-9144-2669 (A.C. Tomás); 0000-0002-4493-8178 (J. Fragata)

Simplified models that closely replicate the outputs of high-fidelity simulations, allow drastic reductions in the calculation time. Thus, surrogate modelling is particularly valuable in scenarios where the extensive reporting time of numerical models imposes a strong practical constraint [11, 12]. In the realm of cardiovascular biomechanics analysis, In this case, surrogate models may be used to increase the efficiency of numerical simulations of ATAAAs biomechanics and, therefore, improve current clinical guidelines. On one hand, numerical model has proved its ability to accurately recreate the conditions of cardiovascular systems, including biological systems [13–16]. On the other hand, surrogate models are able to reduce the computational cost of numerical models, while maintaining an acceptable level of accuracy [11, 17].

Over the past few decades, a variety of techniques have been used to develop surrogate models of biomechanical systems. These techniques vary in complexity and formulation, ranging from classical regression methods to more advanced approaches such as Gaussian process regression [18, 19] and Artificial Intelligence (AI) architectures [20, 21]. Gaussian processes were, for instance, used by Di Achille et al. [22] to assist on the estimations of mechanical parameters of the left ventricular myocardium. Regarding AI-based approaches, Liang et al. [23] trained Deep Neural Networks (DNN) with Computational Solid Mechanics (CSM) data of the aortic wall to estimate the deformation field under a fixed pressure load; Moura et al. [24] developed surrogate models of the pelvic floor dynamics during vaginal delivery using tree-based algorithms (random forests and extreme gradient boosting), support vector regression, and Artificial Neural Networks (ANN). These aimed to estimate the maximum principal stress distribution along the pelvic floor muscle at different stages of fetal head descent; and Sajjadinia et al. [25] used graph neural networks to develop multiscale surrogate models of knee cartilage.

In this chapter, we present a surrogate modelling framework that couples CSM simulations and neural networks to reproduce aortic wall mechanics in patient-specific geometries. This model aims to estimate the Second Piola-Kirchhoff stress and deformation gradient tensors distribution along the aortic wall. The surrogate model is based on a neural network architecture trained with numerical data. We used mesh/morphing techniques and Principal Component Analysis (PCA) to encode the information regarding the aortic geometry. Material and hemodynamic variability was also included through parameters such as wall thickness, Young's modulus, and blood pressure. The remainder of this article is organized as follows: Section 2 details the methodology employed to generate the database of numerical data and train the neural network; Section 3 presents the results of the surrogate model performance; Section 4 discusses the main findings; and Section 5 concludes the chapter with a summary of the contributions.

2. Materials and Methods

The main purpose of this chapter is to develop an AI-based surrogate model of ATAA structural mechanics. In Fig. 1 we present the workflow of the proposed surrogate model which consists in three main steps: (i) statistical shape analysis; (ii) numerical simulations of ATAA wall mechanics; and (iii) AI pipeline.

2.1. Patient-specific anatomy dataset

This work utilized patient-specific Computed Tomography Angiography (CTA) data from 70 individuals diagnosed with ATAAAs, comprising cases with both Bicuspid Aortic Valve (BAV) and Tricuspid Aortic Valve (TAV). All patients were recruited under the scope of the AneurysmTool project (DOI: 10.54499/PTDC/EMD-EMD/1230/2021) and provided written informed consent. The study protocol was approved by the Ethics Committee of the *Unidade Local de Saúde São José*.

The CTA scans were acquired using a Revolution CT scanner (GE Healthcare, Milwaukee, WI, USA) with administration of an iodinated contrast agent (Ultravist 370, Bayer, Leverkusen, Germany), resulting in volumetric datasets of $512 \times 512 \times 292$ voxels, with an isotropic spatial resolution of 0.63 mm. Aortic lumen segmentations were obtained at two phases of the cardiac cycle using a in-house build multi-view 2D U-Net. This method employs three independently trained U-Net encoder-decoder architectures, corresponding to the axial, coronal, and sagittal planes, in order to balance segmentation accuracy and computational efficiency. A total of $K = 94$ segmentations were generated with at least one of each patient. Issues were found in some segmentations and excluded from the study.

Following segmentation, the ascending aorta was geometrically isolated to focus the analysis on this region of interest. This was achieved by slicing the aortic lumen at the sinotubular junction and at the first ostium of the brachiocephalic artery. The extraction process relied on computing the aortic centerline using the inscribed sphere method and Voronoi diagram-based techniques.

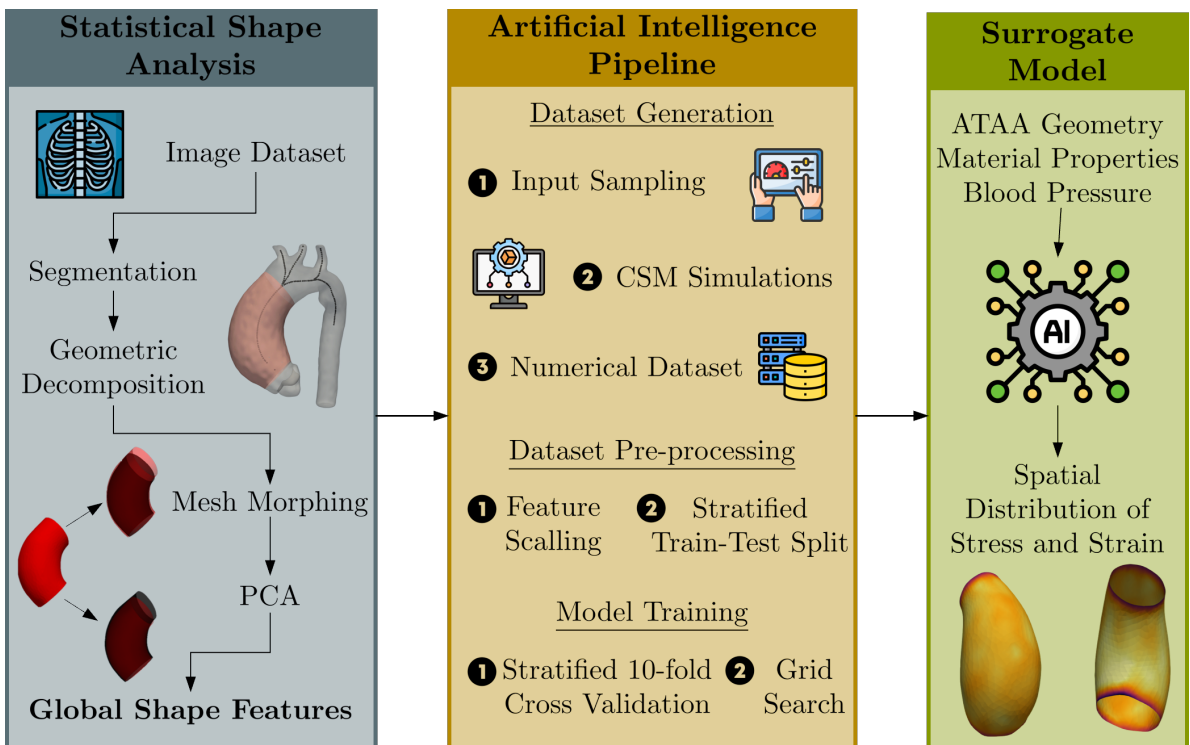


Figure 1: Overview of the methodology employed to develop an AI-based surrogate model of ATAA wall mechanics. Statistical shape analysis was applied to an image dataset to extract global shape features via PCA. These features, combined with material properties and blood pressure, were used to generate a dataset of CSM simulations. The dataset was pre-processed and employed to train the surrogate model using stratified 10-fold cross-validation and grid search. The trained model predicts the spatial distribution of wall stress and strain.

2.2. Mesh morphing

Developing a Statistical Shape Model (SSM) of the ATAA requires generating a set of iso-topological meshes that represent patient-specific anatomies. This was accomplished through a two-step procedure. First, all segmented ATAA surfaces were spatially aligned with a reference mesh using an iterative closest point (Iterative Closest Point (ICP)) algorithm to ensure consistent anatomical orientation. Second, the aligned reference mesh was deformed to fit each target surface using radial basis function mesh morphing. A thin plate spline kernel was selected to interpolate displacements across the 3D domain.

A key challenge in morphing anatomical structures lies in the absence of distinct anatomical landmarks. To address this, we developed an automated approach for extracting pseudo-landmarks—referred to as **Source Pointss** (SPs) to guide the morphing process. These SPs were defined by uniformly sampling previously extracted centerline-based splines along the aortic wall. For each geometry, 16 SPs were selected per spline across 10 cross-sectional planes.

The initial reference mesh was chosen as the surface corresponding to the average ATAA diameter and centerline length across the dataset [26, 27]. A triangular surface mesh was then generated using **A** triangular surface mesh was generated using the TetGen libraries within the SimVascular framework [28], comprising $n = 1354$ elements.

To reduce mesh distortion and improve consistency across the dataset, a refined template was generated by averaging the initially morphed meshes. The entire morphing procedure was then repeated using this mean template as the new reference. This iterative refinement yielded a robust and consistent set of iso-topological meshes for all patient-specific geometries.

2.3. Statistical shape analysis

A statistical shape analysis was conducted on the iso-topological surface meshes to identify global shape features of the ATAA. PCA was employed for this purpose, implemented in Python using the *scikit-learn* library. The resulting

low-dimensional representation enabled compact characterization of each patient-specific geometry and was later used as input for the surrogate model.

The spatial coordinates of each mesh were vectorized by concatenating the x , y , and z components of all n mesh nodes, resulting in a data matrix of size $K \times 3n$. Prior to PCA, the matrix was standardized using the *StandardScaler* function to ensure zero mean and unit variance for each coordinate dimension across the dataset.

PCA was then applied to extract the principal modes of geometric variation. The first six principal components, ranked by decreasing explained variance, were retained for further analysis. Together, these components accounted for around 90% of the cumulative morphological variance in the geometries dataset. The corresponding modes describe major patterns of morphological variation in the ATAA, such as elongation, dilation, and asymmetry.

2.4. Numerical simulations of aortic wall mechanics

The mechanical response of the ATAA wall throughout the cardiac cycle was simulated using CSM simulations. The primary objective was to estimate the spatial distributions of the Second Piola-Kirchhoff stress tensor, \mathbf{S} , and the Right Cauchy-Green strain tensor, \mathbf{C} , under physiological pressure loading. These quantities were later used as output targets for the surrogate model.

The solid domain was generated by extruding the iso-topological surface meshes along the outward normal direction, assuming a uniform wall thickness. The resultant surface mesh of the ATAA wall was then meshed using the Gmsh library. A Python-based pipeline was developed to automate this step, ensuring consistent mesh generation across all patient-specific geometries. Node correspondence was preserved between the surface and volumetric meshes to maintain compatibility with the global shape features extracted through statistical shape analysis.

The aortic wall was modelled as a homogeneous, isotropic, incompressible, Neo-Hookean material. A monolayer structure with constant wall thickness was assumed for all geometries. To better reflect physiological conditions, prestressing was included, following the method described by Hsu and Bazilevs [29]. This approach estimates the prestress tensor required to balance the hemodynamic loads at the diastolic phase, thus estimating the intramural stress state of the aortic wall. As for boundary conditions, a homogeneous pressure load was applied to the luminal surface of the aortic wall. The pressure values followed an idealized curve. At the proximal and distal extremities of the domain, the displacements were fixed.

All simulations were carried out using SimVascular on a workstation equipped with an Intel Xeon Gold 6242R 3.10 GHz CPU and 40 cores. A total of 4000 simulations were attempted, of which 3911 were successfully completed. The aortic wall density and Poisson's ratio were fixed at 1120 kg m^{-3} [30, 31] and 0.49 [32, 33], respectively. Computational settings, including the time step size and number of time steps, were kept constant across all simulations. The varying variables included the wall thickness and Young's modulus, sampled from uniform distributions $U(1, 2.5) \text{ mm}$ [34] and $U(1, 4) \text{ MPa}$ [35], respectively. The diastolic and systolic pressures also varied and the followed normal distributions $N(80, 16) \text{ mmHg}$ and $N(120, 16) \text{ mmHg}$, respectively.

In addition to varying mechanical and loading parameters, 500 ATAA geometries were synthetically generated by sampling the first six PCA modes. Each mode was sampled from a normal distribution with zero mean and variance equal to the corresponding eigenvalue of the PCA covariance matrix, enabling the creation of anatomically plausible yet diverse shapes for the simulation campaign.

2.5. Artificial intelligence pipeline

2.5.1. Dataset generation

The dataset used to train the surrogate model was constructed from the results of the CSM simulations described previously. From each simulation, 20 samples were extracted, corresponding to 20 different loading states throughout the cardiac cycle. Each sample was defined by a unique combination of geometry, material properties, and loading conditions, resulting in a total of $m = 78220$ samples.

Each data sample consisted of an input–output pair. The input vector contained 10 features: the first six corresponded to the first six PCA modes, representing the patient-specific geometry. The remaining four included wall thickness, Young's modulus, diastolic pressure, and the instantaneous pressure applied.

The output vector captured the nodal distribution of two tensor fields: the Second Piola-Kirchhoff stress tensor, \mathbf{S} , and the Right Cauchy-Green strain tensor, \mathbf{C} . For each node in the iso-topological mesh, the six unique components of each tensor (due to symmetry) were recorded. As a result, each row of the output dataset had a length of $n \times 12$, with the first half corresponding to the components of \mathbf{S} and the second half to those of \mathbf{C} .

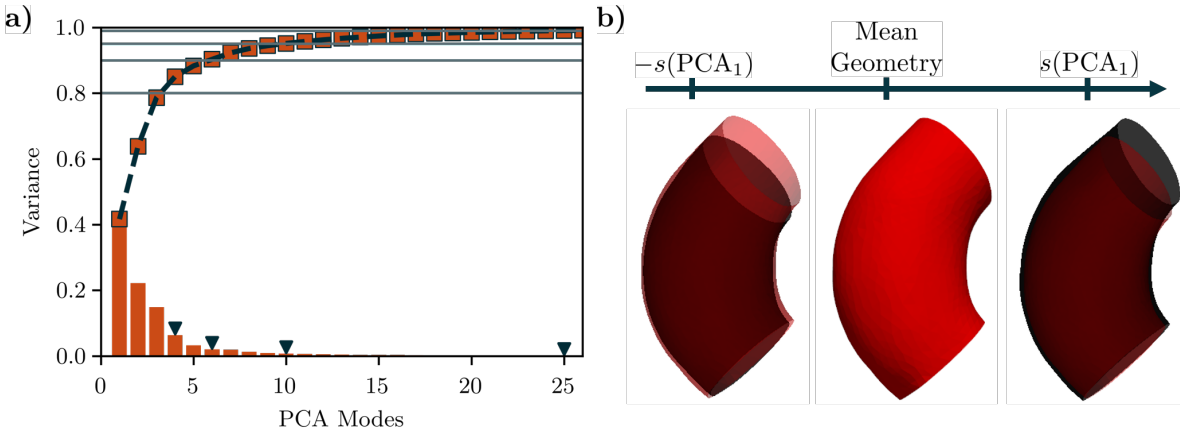


Figure 2: Results of the SSM: a) compactness curve of the PCA (the symbols mark the number of modes required to capture 80 %, 90 %, 95 %, and 99 % of the cumulative variance), and b) geometric variations imposed by the first PCA mode on the mean shape (bright red).

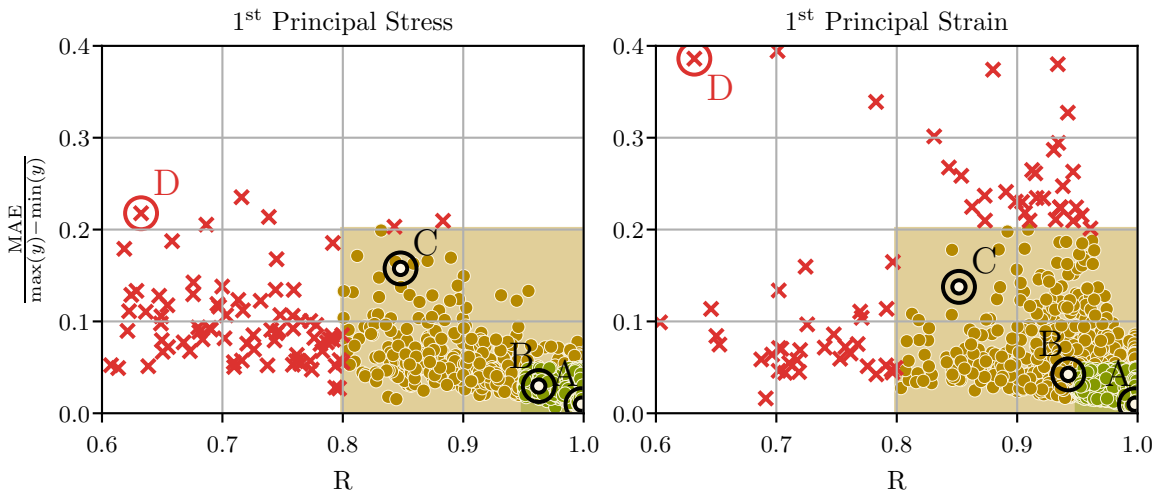


Figure 3: DNN performance overview: summary of the NMAE and R for all test samples.

2.5.2. Data pre-processing

To improve the robustness of the training process and ensure balanced data distribution across training, validation and testing splits, a stratified sampling strategy was employed. Specifically, the dataset was clustered into clusters using the *KMeans* algorithm, based on the input features. These clusters were then used to perform a stratified shuffle split via the *StratifiedShuffleSplit* function from the *scikit-learn* library. The data was divided into training (80%) and testing (20%) sets. Within the training set, an additional 10% was reserved for validation, resulting in final proportions of 72% for training, 8% for validation, and 20% for testing.

All input features were standardized using the *StandardScaler* from *scikit-learn*, applied only to the training data to avoid data leakage. This process ensures that each feature has zero mean and unit variance. The scaling parameters computed from the training set were then used to transform both the validation and testing sets, maintaining consistency across the datasets. Additionally, this transformation was performed independently for groups of variables with the same order of magnitude, ensuring that each group was scaled to have zero mean and unit variance. For instance, the PCAs modes were scaled together, while the wall thickness, Young's modulus, and pressure values were scaled separately.

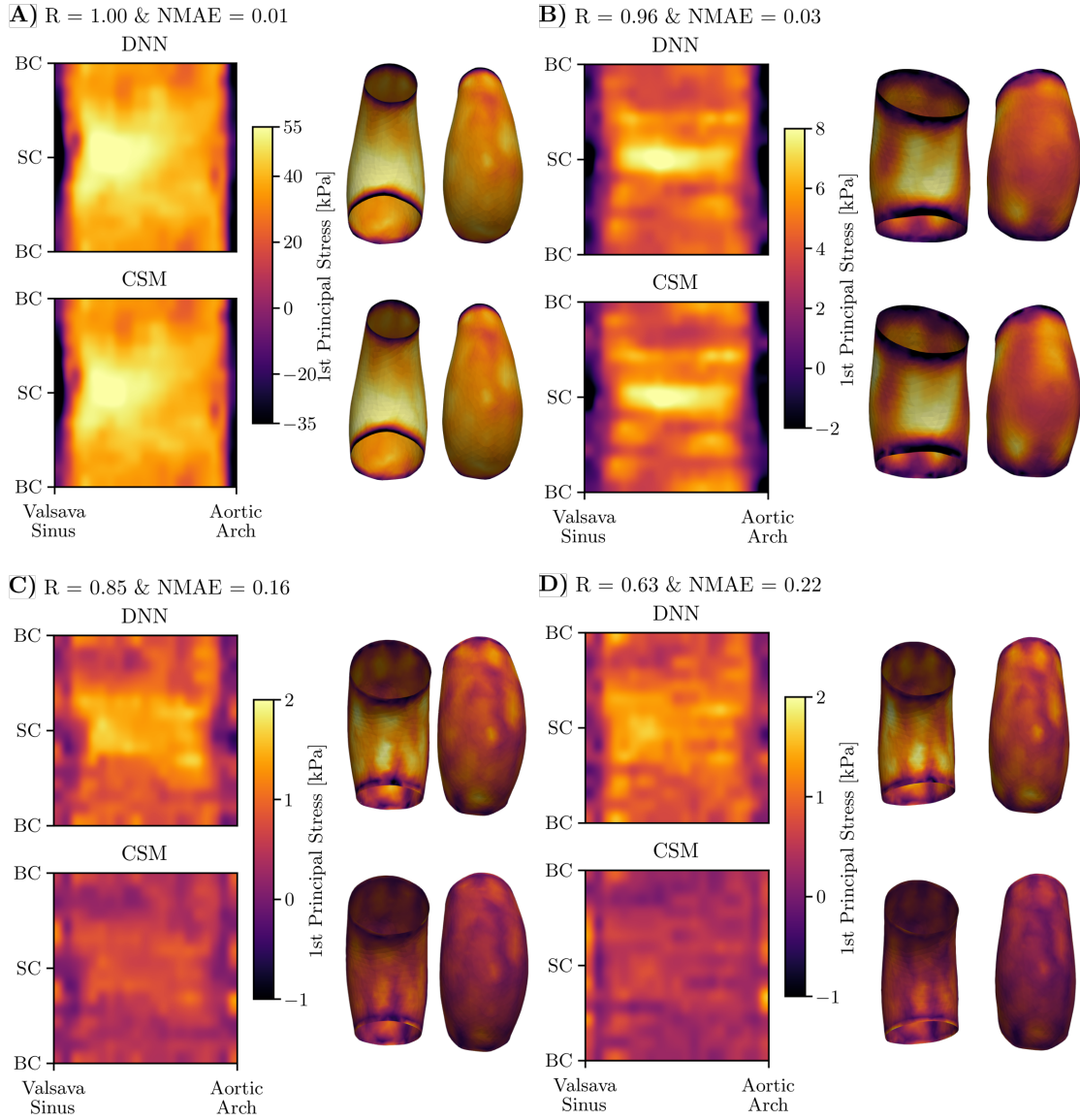


Figure 4: Surface representation of the surrogate and CSM model predictions of the first principal stress.

2.5.3. Model training

To perform regression operations, in particular when coupling CSM data and Machine Learning (ML), neural networks are the most commonly used approach [36]. There are also known for being capable of handling nonlinear relationships between high-dimensional input and output data [37]. This is particularly relevant, as the developed model aims to estimate the nodal distribution of the Second Piola-Kirchhoff stress and Right Cauchy-Green strain tensors. Also, this model was implemented using the *PyTorch* framework.

To identify the optimal set of hyperparameters, a grid search (*GridSearchCV*) strategy was employed in combination with stratified 10-fold cross-validation (*StratifiedKFold*). The grid search exhaustively evaluated combinations over a predefined parameter space, including learning rate, number of hidden layers, number of neurons per layer, dropout rate, and batch size. The final hyperparameters used for training are summarized in Table 1.

The loss function used during training was suggested by Ghazi et al. [38], which aims to penalize more for elements with higher variation across the training samples. The loss function is as follows:

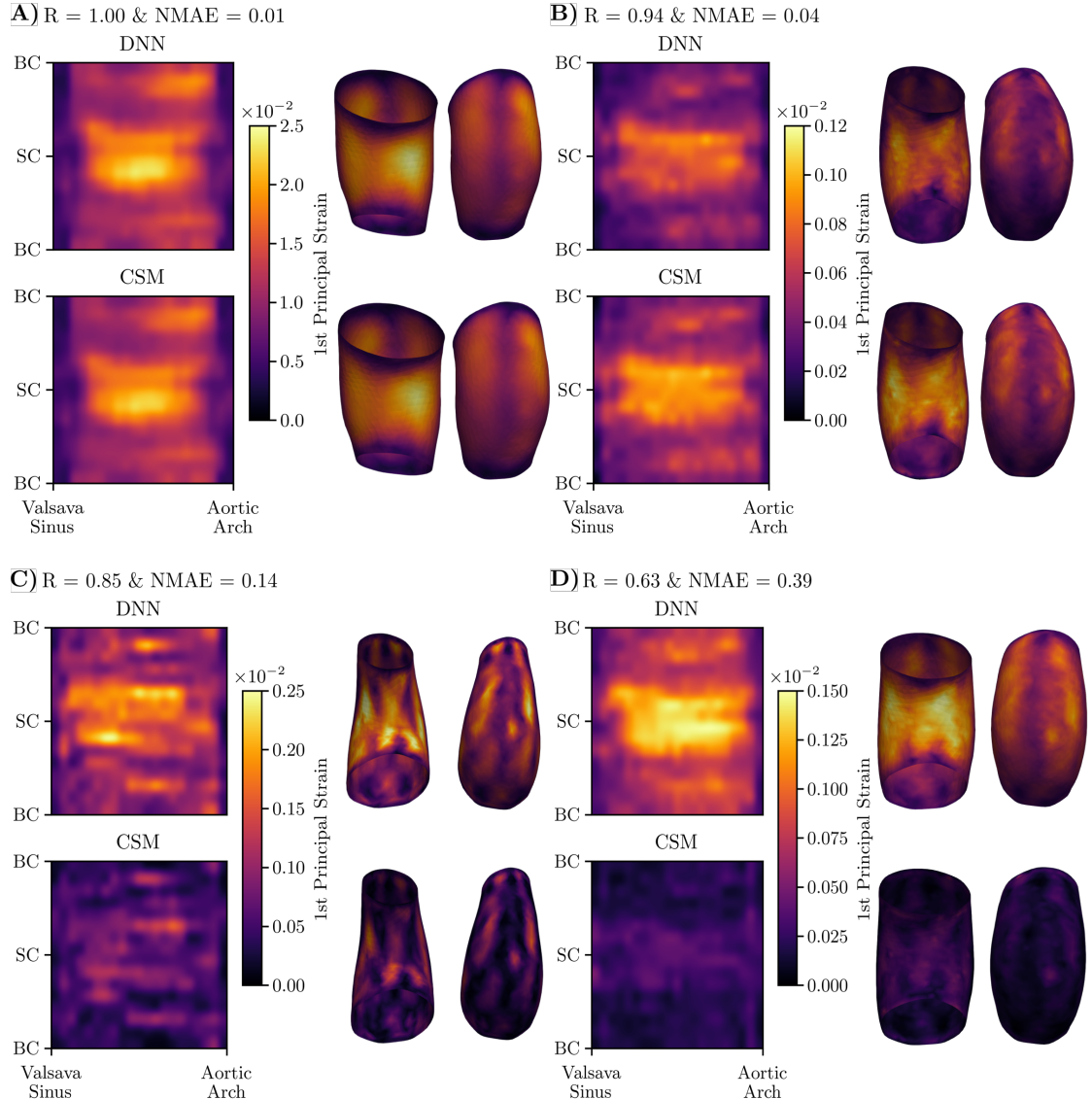


Figure 5: Surface representation of the surrogate and CSM model predictions of the first principal strain.

$$\text{loss} = \frac{1}{n \times m} \sum_{i=1}^n \left(\sum_{j=1}^m s_i (y_j - \hat{y}_j)^2 \right) \quad (1)$$

where n is the number of nodes, m is the number of samples, s_i is the standard deviation of the i -th node across all samples, y_i is the true value at the i -th node, and \hat{y}_i is the predicted value at the same node.

2.5.4. Performance metrics

To evaluate the performance of the trained neural networks, two metrics were computed across all testing samples: the normalized mean absolute error, NMAE, and the Pearson correlation coefficient, R. The NMAE was computed as:

Table 1

Final hyperparameters used in the training of the surrogate model.

Hyperparameter	Value
Hidden layers	64, 128, 256, 512, 1024
Activation function	ReLU
Batch size	400
Optimizer	Adam
Dropout rate	0.2
Epochs	152

$$\text{NMAE} = \frac{1}{m} \sum_{i=1}^m \frac{|y_i - \hat{y}_i|}{\max(y_i) - \min(y_i)} \quad (2)$$

These metrics were estimated independently for the predicted distributions of Second Piola-Kirchhoff stress (\mathbf{S}) and Right Cauchy-Green strain (\mathbf{C}). Additionally, the same analysis was repeated for the subset of patient-specific ATAA geometries. To better access the performance of the surrogate model, two thresholds for success were defined:

- Moderate agreement: $R > 0.8$ and $\text{NMAE} < 0.2$
- High agreement: $R > 0.95$ and $\text{NMAE} < 0.05$

3. Results

3.1. PCA results

Concerning the results of the SSM, Fig. 2-a shows the compactness curve. The first mode alone captures approximately 42 % of the anatomical variation in the sample of patient-specific geometries characterized with isotopological meshes. The Second and third modes represent 22 % and 15 %, respectively. Together, these three modes account for nearly 80 % of the variability. The 90 %, 95 %, and 99 % thresholds of the compactness curve were reached using 6, 10, and 25 PCA modes, respectively. Fig. 2-b illustrates the changes in geometry obtained by varying the first PCA mode around the mean shape.

3.2. Neural network performance

3.2.1. Case 1 – PCA-driven geometries

Fig. 3 summarizes the NMAE and R of all test samples. For the predictions of the Second Piola-Kirchhoff stress tensor components, 99 % and 96 % of the samples showed a moderate and high agreement, respectively. For the predictions of the Right Green-Cauchy strain tensor, 99 % and 95 % of the samples fell into these categories, respectively.

Fig. 4 and Fig. 5 present the surface representations of the first principal stress and strain for four representative test cases. These examples cover different levels of agreement between the surrogate model predictions and the CSM simulations: A) very high, B) high, C) moderate, and D) low agreement. The heatmaps illustrate the spatial distribution in the ascending aorta mapped into a topologically equivalent rectangle. The y-axis corresponds to the circumferential direction, with BC and SC denoting the big and small curvatures, respectively, while the x-axis corresponds to the axial direction.

For stress predictions, across all agreement levels the estimated and reference results exhibit similar spatial distributions. In particular, cases A and B also present a close match in magnitude. Cases C and D show an overestimation of stress magnitudes compared with the reference values. The predictions of the first principal strain follow the same trend, with the overestimation in cases C and D appearing even more pronounced.

3.2.2. Case 2 – Patient-specific geometries

The performance of the surrogate model was also evaluated using the set of patient-specific anatomies employed in the PCA analysis. Figs. 6 and 7 illustrate the comparison between surrogate model predictions and reference CSM

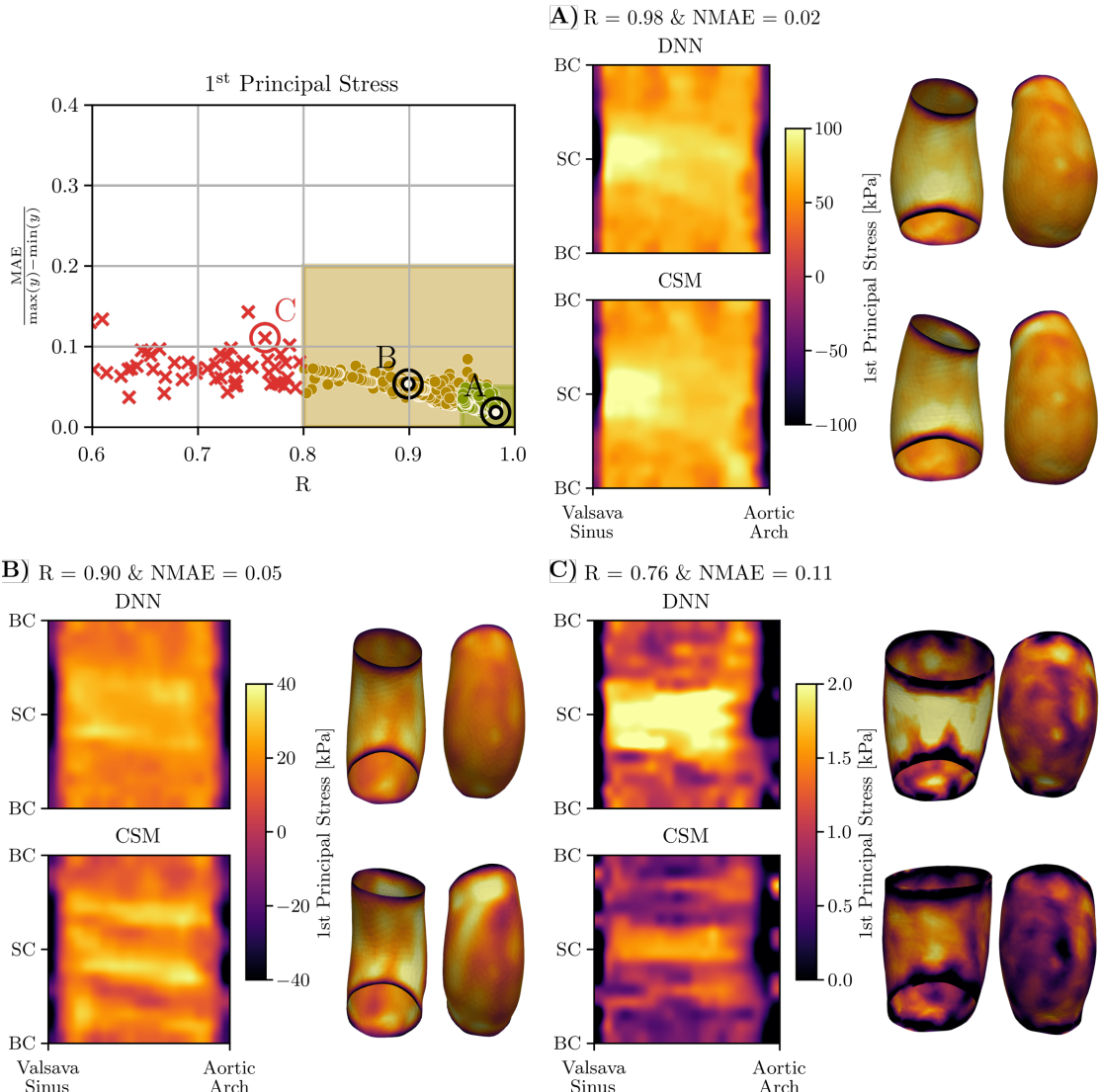


Figure 6: Surface representation of the surrogate and CSM model predictions of the first principal stress for the patient-specific anatomy dataset.

results for the first principal stress and strain, respectively. These figures follow the same rationale as in Case 1, including both the performance overview and the surface representation analysis.

For the patient-specific geometry dataset, the success rates for high agreement changed notably: 51 % and 64 % for the predictions of the Second Piola-Kirchhoff stress and Right Green-Cauchy strain, respectively. Nonetheless, the success rates for moderate agreement remained similar (95 % and 97 %, respectively). As with the PCA-driven cases, the DNN predicted spatial distributions follow the same qualitative patterns as the CSM simulations. However, more pronounced differences in the magnitude of the variables are observed in regions of reduced mechanical loading.

3.3. Correlation between error and inputs

Fig. 8 examines how the prediction error of the surrogate model varies with different input parameters. The most noticeable trend is observed for the instantaneous pressure: as the pressure increases, the prediction error decreases significantly. For the remaining variables, including the PCA shape modes, wall thickness, and Young's modulus, no clear or consistent relationship with the error can be identified.

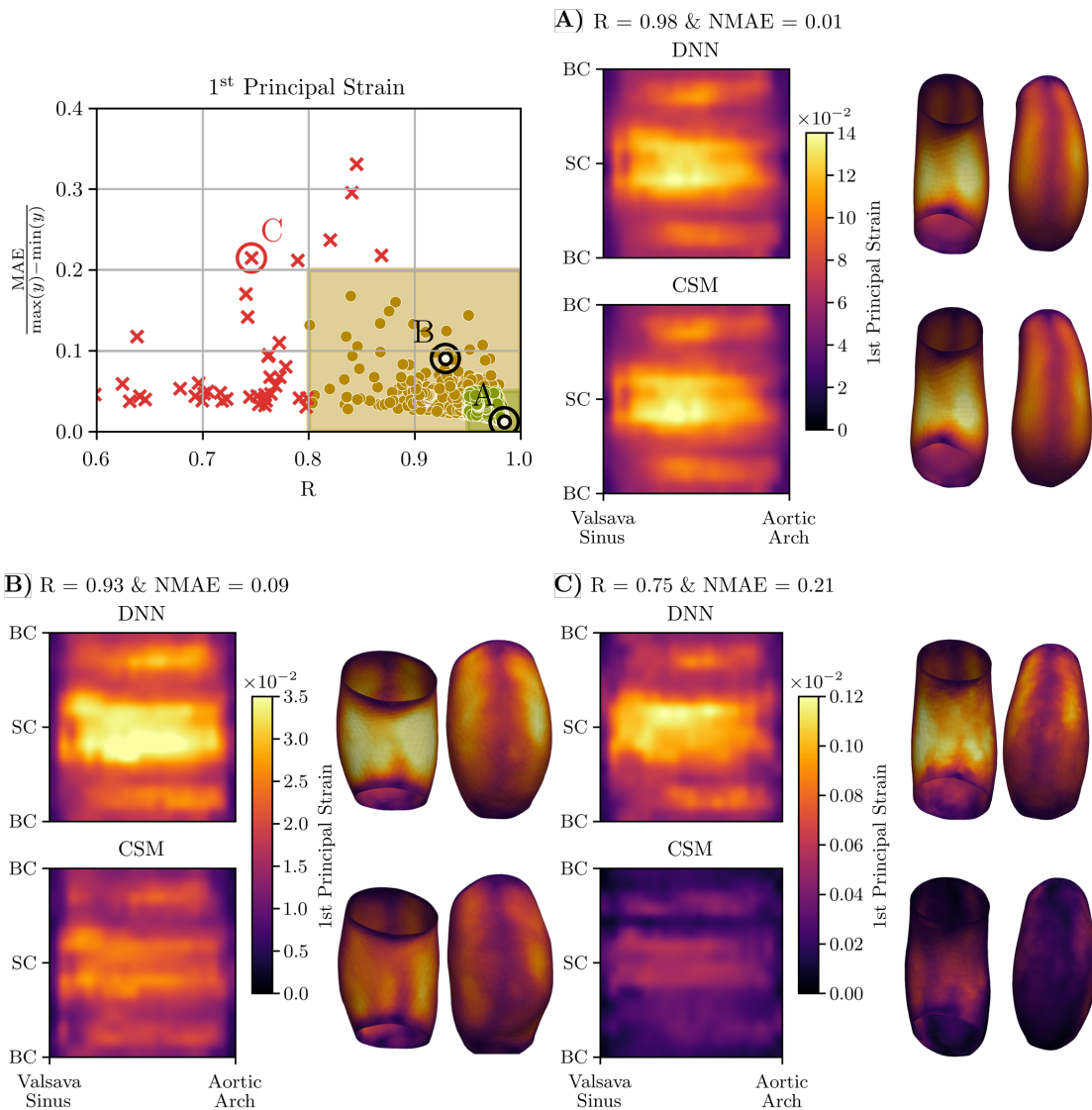


Figure 7: Surface representation of the surrogate and CSM model predictions of the first principal strain for the patient-specific anatomy dataset.

4. Discussion

The work presented in this chapter introduced a surrogate modeling framework for predicting the mechanical response of ATAA. By combining SSM, CSM simulations, and DNNs, we developed a tool capable of reproducing the spatial distribution of the Second Piola-Kirchhoff and Right Cauchy-Green tensors with good agreement to reference simulations. The model showed robust generalization across the input space, with its main sensitivity being associated with the loading conditions. In particular, prediction accuracy improved at higher instantaneous pressures, indicating that the surrogate performs more reliably under high loading conditions, such as peak systolic pressure.

One of the most relevant outcomes of this study is the gain in reporting time. While the reference CSM simulations required between 20–60 minutes to complete on a high-performance workstation, the surrogate model generated results in less than one second on a low-end computer. This substantial reduction in computational demand highlights the clinical potential of such approaches, where time-efficient tools are essential. The computational burden is transferred almost entirely to the training stage, enabling rapid deployment once the model is trained. Nonetheless, a limitation

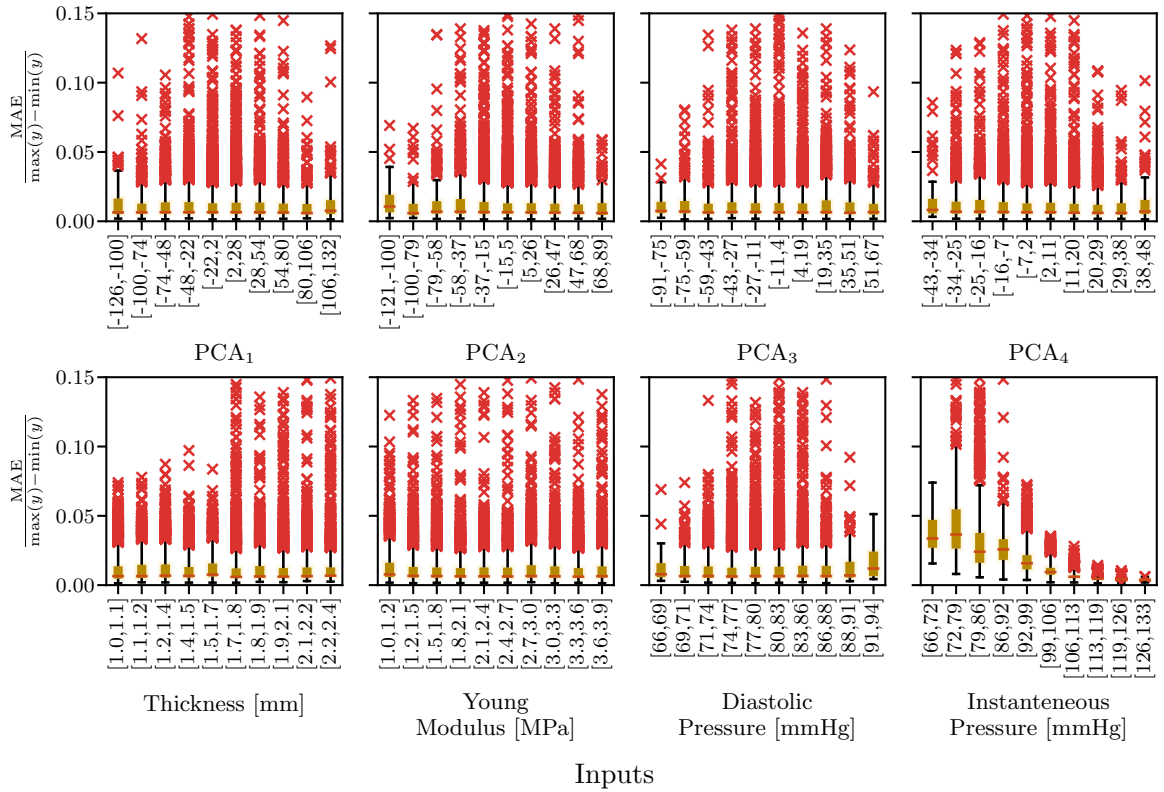


Figure 8: Correlation between the NMAE of the surrogate model predictions and the input parameters.

of this strategy is the need for retraining whenever significant changes are introduced, such as new input features. Retraining the surrogate model may also require performing new simulations, for instance if boundary conditions are altered.

The performance analysis also revealed a decrease in success rate when the surrogate was applied to patient-specific anatomies, when compared to PCA-driven geometries. This reduction underscores the importance of expanding the input space to better capture anatomical variability. As future work, training the model with a higher number of PCA modes (for instance, the first 25 modes, which describe 99% of the shape variability) may improve predictive performance for patient-specific cases. Although this study focused on the ascending aorta, the proposed methodology could be extended to the full aortic geometry. Achieving this goal will require the development of more efficient mesh morphing strategies, capable of handling the increased anatomical complexity.

Additional improvements can also be made in the constitutive description of the aortic wall. The present framework assumes a homogeneous wall with constant thickness and material properties. More physiologically realistic descriptions, such as spatially varying thickness, heterogeneous material properties, and histo-mechanical constitutive models, would better capture the underlying biomechanics. Incorporating these features, together with numerical validation, will be key steps towards building clinically reliable digital twins of aortic aneurysms. Future work may also include training the effects of hypertension and hypotension.

5. Conclusion

One of the main bottlenecks limiting the introduction of numerical models of ATAA biomechanics is the long computational time required for patient-specific analyses. Deep Learning architectures trained on numerical simulation data offer a promising approach to overcome this limitation, as demonstrated in the present work. In this chapter, a surrogate model of ATAA wall mechanics was proposed, combining a SSM, DNN, and CSM simulations. The surrogate model was able to reproduce the spatial distributions of the Second Piola-Kirchhoff and Right Green-Cauchy

tensors across almost the entire test dataset. For the patient-specific geometries, more than 95 % of the predictions reached at least moderate agreement, confirming the robustness of the approach. Overall, this chapter demonstrates the feasibility and impact of using data-driven surrogate modeling to accelerate patient-specific biomechanical analyses, representing a significant step toward clinical translation.

Acknowledgments

This research was funded by the Portuguese Foundation for Science and Technology (FCT,IP) under the projects: “Fluid-structure interaction for functional assessment of ascending aortic aneurysms: a biomechanical-based approach toward clinical practice” (AneurysmTool) DOI: 10.54499/PTDC/EMD-EMD/1230/2021; UNIDEMI: UIDB/00667/2020 and UIDP/00667/2020; A. Mourato Ph.D. grant DOI:10.54499/UI/BD/151212/2021, R. Valente Ph.D. grant 2022.12223.BD.

CRediT authorship contribution statement

André Mourato: Conceptualization, Methodology, Software, Validation, Formal analysis, Investigation, Data curation, Writing - Original Draft, Visualization. **Rodrigo Valente:**  Writing - Review & Editing. **José Xavier:** Conceptualization, Methodology, Validation, Resources, Writing - Review & Editing, Supervision, Project administration, Funding acquisition. **Moisés Brito:** Conceptualization, Methodology, Validation, Resources, Writing - Review & Editing, Supervision. **Stéphane Avril:** Conceptualization, Methodology, Validation, Resources, Writing - Review & Editing, Supervision. **António C. Tomás:** Writing - Review & Editing. **José Fragata:** Writing - Review & Editing, Supervision, Project administration, Funding acquisition.

References

- [1] R. Gouveia e Melo, G. Silva Duarte, A. Lopes, M. Alves, D. Caldeira, R. Fernandes e Fernandes, L. Mendes Pedro, Incidence and prevalence of thoracic aortic aneurysms: A systematic review and meta-analysis of population-based studies, *Seminars in Thoracic and Cardiovascular Surgery* 34 (2022) 1–16.
- [2] G. A. Kuzmik, A. X. Sang, J. A. Elefteriades, Natural history of thoracic aortic aneurysms, *Journal of Vascular Surgery* 56 (2012) 565–571.
- [3] R. Erbel, V. Aboyans, C. Boileau, E. Bossone, R. D. Bartolomeo, H. Eggebrecht, A. Evangelista, V. Falk, H. Frank, et al., 2014 ESC guidelines on the diagnosis and treatment of aortic diseases: document covering acute and chronic aortic diseases of the thoracic and abdominal aorta of the adult the task force for the diagnosis and treatment of aortic diseases of the European Society of Cardiology (ESC), *Eur. Heart J.* 35 (2014) 2873–2926.
- [4] L. F. Hiratzka, G. L. Bakris, J. A. Beckman, R. M. Bersin, V. F. Carr, D. E. Casey, K. A. Eagle, L. K. Hermann, E. M. Isselbacher, E. A. Kazerooni, N. T. Kouchoukos, B. W. Lytle, D. M. Milewicz, D. L. Reich, S. Sen, J. A. Shinn, L. G. Svensson, D. M. Williams, 2010 ACCF / AHA / AATS / ACR / ASA / SCA / SCAI / SIR / STS / SVM guidelines for the diagnosis and management of patients with thoracic aortic disease, *J. Am. Coll. Cardiol.* 55 (2010) e27–e129.
- [5] G. Martufi, A. Forneris, J. J. Appoo, E. S. Di Martino, Is there a role for biomechanical engineering in helping to elucidate the risk profile of the thoracic aorta?, *The Annals of Thoracic Surgery* 101 (2016) 390–398.
- [6] L. A. Pape, T. T. Tsai, E. M. Isselbacher, J. K. Oh, P. T. O’Gara, A. Evangelista, R. Fattori, G. Meinhardt, S. Trimarchi, E. Bossone, T. Suzuki, J. V. Cooper, J. B. Froehlich, C. A. Nienaber, K. A. Eagle, Aortic diameter > or = 5.5 cm is not a good predictor of type A aortic dissection: Observations from the international registry of acute aortic dissection (IRAD), *Circulation* 116 (2007) 1120 – 1127.
- [7] I. Sazonov, A. Khir, W. Hacham, E. Boileau, J. Carson, R. van Loon, C. Ferguson, P. Nithiarasu, A novel method for non-invasively detecting the severity and location of aortic aneurysms, *Biomech. Model. Mechanobiol.* 16 (2017) 1225–1242.
- [8] J. K. Long Ko, R. W. Liu, D. Ma, L. Shi, S. C. Ho Yu, D. Wang, Pulsatile hemodynamics in patient-specific thoracic aortic dissection models constructed from computed tomography angiography, *J. X-Ray Sci. Technol.* 25 (2017) 233–245.
- [9] J. Brunet, B. Pierrat, P. Badel, A parametric study on factors influencing the onset and propagation of aortic dissection using the extended finite element method, *IEEE Trans. Biomed. Eng.* 68 (2021) 2918–2929.
- [10] M.-H. Moosavi, N. Fatouraei, H. Katoozian, A. Pashaei, O. Camara, A. Frangi, Numerical simulation of blood flow in the left ventricle and aortic sinus using magnetic resonance imaging and computational fluid dynamics, *Comput. Methods Biomed. Eng.* 17 (2014) 740–749.
- [11] R. Alizadeh, J. K. Allen, F. Mistree, Managing computational complexity using surrogate models: a critical review, *Research in Engineering Design* 31 (2020) 275–298.
- [12] V. Mendez, M. Di Giuseppe, S. Pasta, Comparison of hemodynamic and structural indices of ascending thoracic aortic aneurysm as predicted by 2-way FSI, CFD rigid wall simulation and patient-specific displacement-based FEA, *Comput. Biol. Med.* 100 (2018) 221–229.
- [13] A. Mariotti, A. Boccadifuccio, S. Celi, M. Salvetti, Hemodynamics and stresses in numerical simulations of the thoracic aorta: Stochastic sensitivity analysis to inlet flow-rate waveform, *Comput. Fluids* 230 (2021) 173–182.
- [14] J. Bols, L. Taelman, G. De Santis, J. Degroote, B. Verheghe, P. Segers, J. Vierendeels, Unstructured hexahedral mesh generation of complex vascular trees using a multi-block grid-based approach, *Comput. Methods Biomed. Eng.* 19 (2016) 663–672.

- [15] A.-S. Yang, C.-Y. Wen, L.-Y. Tseng, C.-C. Chiang, W.-Y. Tseng, H.-Y. Yu, An innovative numerical approach to resolve the pulse wave velocity in a healthy thoracic aorta model, *Comput. Methods Biomed. Eng.* 17 (2014) 461–473.
- [16] J. Lantz, J. Renner, M. Karlsson, Wall shear stress in a subject specific human aorta - influence of fluid-structure interaction, *Int. J. Appl. Mech.* 3 (2011) 759–778.
- [17] S. Donmazov, E. N. Saruhan, K. Pekkan, S. Piskin, Review of machine learning techniques in soft tissue biomechanics and biomaterials, *Cardiovascular Engineering and Technology* (2024) 1–28.
- [18] G. Su, L. Peng, L. Hu, A gaussian process-based dynamic surrogate model for complex engineering structural reliability analysis, *Struct. Saf.* 68 (2017) 97–109.
- [19] T. Saida, M. Nishio, Transfer learning gaussian process regression surrogate model with explainability for structural reliability analysis under variation in uncertainties, *Comput. Struct.* 281 (2023) 107014.
- [20] A. Hashemi, J. Jang, J. Beheshti, A machine learning-based surrogate finite element model for estimating dynamic response of mechanical systems, *IEEE Access* 11 (2023) 54509–54525.
- [21] R. Moura, D. A. Oliveira, J. P. S. Ferreira, M. P. L. Parente, N. Kimmich, R. M. Natal Jorge, A finite element-based machine learning framework to predict the mechanical behavior of the pelvic floor muscles during childbirth, *Expert Syst. Appl.* 250 (2024) 123953.
- [22] P. Di Achille, A. Harouni, S. Khamzin, O. Solovyova, J. J. Rice, V. Gurev, Gaussian process regressions for inverse problems and parameter searches in models of ventricular mechanics, *Front. Physiol.* 9 (2018) 1002.
- [23] L. Liang, M. Liu, J. Elefteriades, W. Sun, Synergistic integration of deep neural networks and finite element method with applications of nonlinear large deformation biomechanics, *Comput. Methods Appl. Mech. Eng.* 416 (2023) 116347.
- [24] R. Moura, D. A. Oliveira, M. P. L. Parente, N. Kimmich, L. Hynčík, L. H. Hympánová, R. M. N. Jorge, Patient-specific surrogate model to predict pelvic floor dynamics during vaginal delivery, *J. Mech. Behav. Biomed. Mater.* 160 (2024) 106736.
- [25] S. S. Sajjadinia, B. Carpentieri, G. A. Holzapfel, Bridging diverse physics and scales of knee cartilage with efficient and augmented graph learning, *IEEE Access* 12 (2024) 86302–86318.
- [26] L. Gerloni, A. Martinez, M. Rochette, K. Yan, A. Bel-Brunon, P. Haigron, P. Escrig, J. Tomasi, M. Daniel, A. Lalande, S. Lin, D. M. Marin-Castrillon, O. Bouchot, J. Porterie, P. P. Valentini, M. E. Biancolini, Computer-aided shape features extraction and regression models for predicting the ascending aortic aneurysm growth rate, *Comput. Biol. Med.* 162 (2023) 107052.
- [27] L. Grassi, N. Hraiech, E. Schileo, M. Ansaldi, M. Rochette, M. Viceconti, Evaluation of the generality and accuracy of a new mesh morphing procedure for the human femur, *Medical Engineering & Physics* 33 (2011) 112–120.
- [28] A. Updegrove, N. M. Wilson, J. Merkow, H. Lan, A. L. Marsden, S. C. Shadden, Simvascular: an open source pipeline for cardiovascular simulation, *Ann. Biomed. Eng.* 45 (2017) 525–541.
- [29] M.-C. Hsu, Y. Bazilevs, Blood vessel tissue prestress modeling for vascular fluid–structure interaction simulation 47 (????) 593–599.
- [30] S. Pasta, A. Rinaudo, A. Luca, M. Pilato, C. Scardulla, T. G. Gleason, D. A. Vorp, Difference in hemodynamic and wall stress of ascending thoracic aortic aneurysms with bicuspid and tricuspid aortic valve, *J. Biomech.* 46 (2013) 1729–1738.
- [31] S. Attaran, H. Niroomand-oscui, F. Ghalichi, A novel, simple 3D/2D outflow boundary model for blood flow simulations in compliant arteries, *Comput. Fluids* 174 (2018) 229–240.
- [32] S. Farzaneh, O. Trabelsi, S. Avril, Inverse identification of local stiffness across ascending thoracic aortic aneurysms, *Biomech. Model. Mechanobiol.* 18 (2019) 137–153.
- [33] K. Bäumler, V. Vedula, A. Sailer, J. Seo, P. Chiu, G. Mistelbauer, F. Chan, M. Fischbein, A. Marsden, D. Fleischmann, Fluid–structure interaction simulations of patient-specific aortic dissection, *Biomech. Model. Mechanobiol.* 19 (2020) 1607–1628.
- [34] B. Mensel, A. Quadrat, T. Schneider, J.-P. Kühn, M. Dörr, H. Völzke, W. Lieb, K. Hegenscheid, R. Lorbeer, MRI-based determination of reference values of thoracic aortic wall thickness in a general population, *European Radiology* 24 (2014) 2038–2044.
- [35] A. Duprey, K. Khanafer, M. Schlicht, S. Avril, D. Williams, R. Berguer, In vitro characterisation of physiological and maximum elastic modulus of ascending thoracic aortic aneurysms using uniaxial tensile testing, *European Journal of Vascular and Endovascular Surgery* 39 (2010) 700–707.
- [36] R. Phellan, B. Hachem, J. Clin, J.-M. Mac-Thiong, L. Duong, Real-time biomechanics using the finite element method and machine learning: Review and perspective, *Medical Physics* 48 (2021) 7–18.
- [37] L. Liang, M. Liu, C. Martin, W. Sun, A deep learning approach to estimate stress distribution: a fast and accurate surrogate of finite-element analysis, *Journal of The Royal Society Interface* 15 (2018) 20170844.
- [38] K. Ghazi, S. Wu, W. Zhao, S. Ji, Instantaneous whole-brain strain estimation in dynamic head impact, *Journal of Neurotrauma* 38 (2021) 1023–1035.